Rigaku

X-ray Diffraction & Elemental Analysis

THE BRIDGE

MATERIALS ANALYSIS eNEWSLETTER
APRIL 2014, ISSUE 10

Welcome

This month we are highlighting the fine work being done at the University of Southampton in developing new methodologies for teaching diffraction. Utilizing an electronic notebook to both instruct students and to record their results, Dr. Simon Coles and graduate student Lucy Mapp have developed a course that teaches powder diffraction and single crystal diffraction through a hands-on lab practical.

Rigaku is proud to introduce our new HyPix-3000 semiconductor detector. Based on state-of-the-art pixel array detector technology, the HyPix-3000 two-dimensional detector is the first in a series of detectors that will be optimized for specific diffraction and scattering applications. A particularly useful feature is the ability to use the same detector to operate in 0D, 1D or 2D mode.

For our XRF customers, we are proud to announce our new holderless sample handling system for our ZSX Primus WDXRF spectrometer. For samples that are amenable, this new option gives our customers a technique that reduces sample preparation time as well as allowing increased sample capacity on the deck.

Enjoy the newsletter.

A bridge is often used to symbolize a connection or link between two places, and thus we felt The Bridge would be the perfect name for our eNewsletter, as we hope that it will act as a vehicle for the transmission of ideas and information between Rigaku and interested readers around the world.

And a bridge is a two-way structure, a concept that we will keep in mind as we not only provide information about Rigaku, but also report on interesting research and the associated laboratories around the world, publish technical book reviews that might help our readers in their work, and highlight general news topics that are of interest to many people involved in materials analysis.

Photo by Paul Swepston

Featured Interview

Cameron Chai from AZoM speaks to Joseph Ferrara, VP of the X-Ray Research Laboratory at Rigaku, about their new nano3DX X-ray microscope to find out what it is, what it does and to whom it will be of use.

Rigaku's nano3DX is a true X-ray microscope (XRM) with the ability to measure relatively large samples at high resolution. This is accomplished by using a high powered rotating anode X-ray source and a high-resolution CCD imager. The rotating anode provides for fast data acquisition and the ability to switch anode materials easily to optimize the data acquisition.

Click here to read the interview

The world's most versatile home lab diffraction detector

4 Reasons why the HyPix-3000 detector belongs in your research lab

- Ultra-high dynamic range and high sensitivity
- Seamless switching from 2D-TDI (Time Delay and Integration) mode to 2D snapshot mode to 1D-TDI mode to 0D mode with a single detector
- XRF suppression by high and low energy discrimination
- High spatial resolution, direct-detection pixel array detector

State of the art detector technology

Rigaku's HyPix-3000 is a next-generation two-dimensional semiconductor detector designed specifically to meet the needs of the home lab diffractionist. One of the HyPix-3000's unique features is its large active area of approximately 3000 mm^2 with a small pixel size of 100 µm square, resulting in a detector with high spatial resolution. In addition, the HyPix-3000 is a single photon counting X-ray detector with a high count rate of greater than 10^6 cps/pixel, a fast readout speed and essentially no noise.

Featuring a double-threshold (window) discriminator, the HyPix-3000 has three readout modes that can be selected based on the purpose of a measurement. "Differential" mode can be used to suppress fluorescence from elements in a sample or background derived from cosmic rays. "31-bit" mode is used for experiments in which a very wide dynamic range is needed. "Zero dead time" mode makes it possible to perform extremely fast data collection.

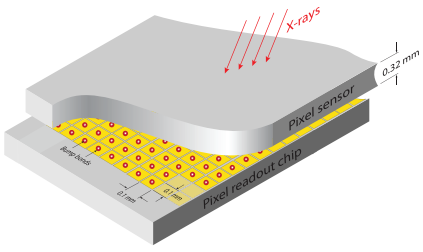

Figure 1. Schematic view of hybrid pixel array detector

The HyPix-3000 was designed for optimal flexibility; for example, the compact angular enclosure was designed to allow excellent high angle accessibility. Compared to the design of other types of detectors, the HyPix-3000 is essentially maintenance free. It does not require an external cooling device, as required on CCD detectors, or gas exchange and anode wire washing, as required on multi-wire detectors.

How do you most effectively suppress background noise?

Each pixel on the HyPix-3000 detector has dual energy discriminators, which makes it possible to adjust the energy window width by setting the energy threshold to "high" and "low", respectively. The low-energy discriminator can eliminate electrical noise and reduce fluorescence background, and the high-energy discriminator can eliminate cosmic rays and white radiation. As a result, you can measure data with an optimized signal-to-noise ratio. Figure 2 shows the X-ray diffraction pattern of a powder sample containing iron measured in standard mode (upper) and XRF reduction mode (lower). By using differential XRF reduction, it is possible to obtain an X-ray diffraction pattern with low background, and thereby improve the ability to detect trace components, even when measuring Fe-based compounds with a Cu source.

Figure 2. X-ray diffraction patterns of iron oxide powder, measured in standard mode and XRF reduction mode

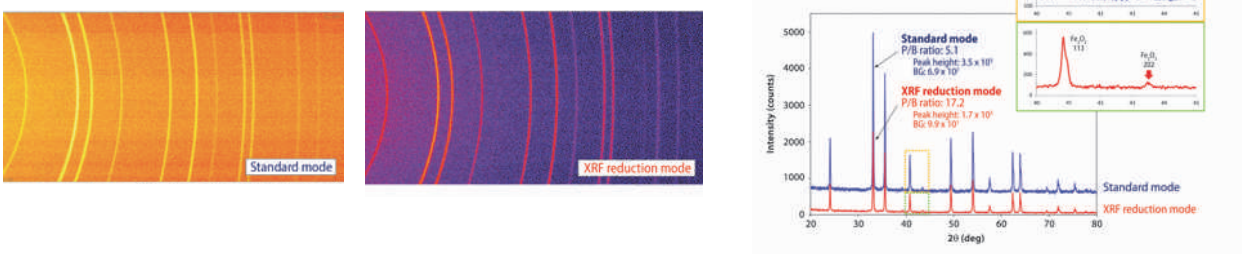

What is the best way to measure very strong reflections?

A big advantage of a hybrid pixel array detector is that each pixel is independent and the overall dynamic range of a detector is a sum of the dynamic range of each individual pixel. Each pixel of the HyPix-3000 has two 16-bit counters, and these can be combined to work as a single 31-bit counter, achieving very wide dynamic range. This means that wide dynamic range measurements can be performed without an attenuator, thus removing the error associated with the attenuator factor, as well as optimizing data measurement time. Figure 3 shows the high-resolution rocking curve profiles of InGaN/GaN multiple quantum wells (MQW) with the HyPix-3000 (wide dynamic range 31-bit mode) and scintillation counter. The profile obtained in 31-bit mode clearly indicates separated peaks without saturation.

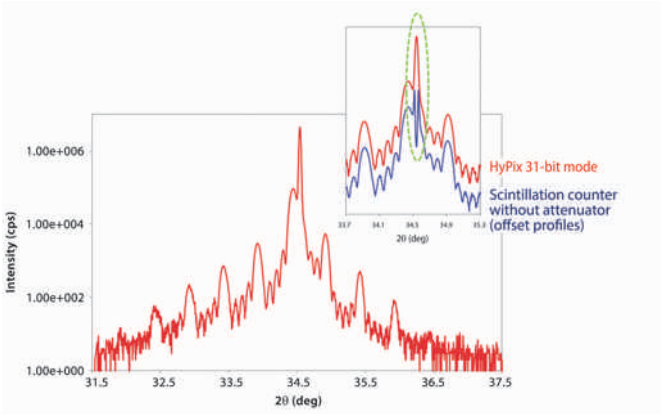

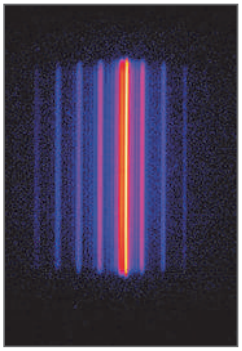

Two-dimensional diffraction image of InGaN/GaN MQW

Figure 3. High resolution rocking curve profiles of InGaN/GaN MQW

How do you obtain data with excellent spatial resolution?

The HyPix-3000 detector's small pixel size provides outstanding spatial resolution. Figure 4 shows a typical qualitative analysis, which, in this example, was done in 2 minutes. In this case, the detector was run in a one dimensional Time Delay and Integration mode (1D-TDI mode), which allows continuous movement of the detector during measurement. If you want resolution less than 0.03 degrees at full width at half maximum (FWHM), as shown in Figure 5, you can run the detector in 0D mode which requires placing a mechanical slit on the face of the detector.

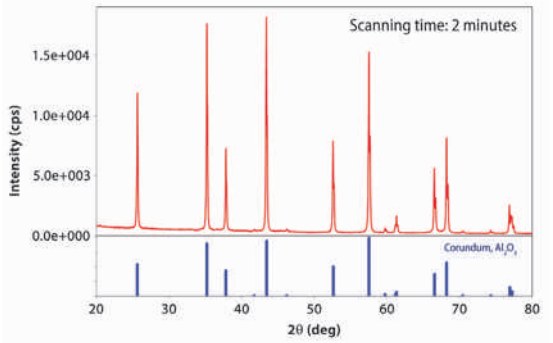

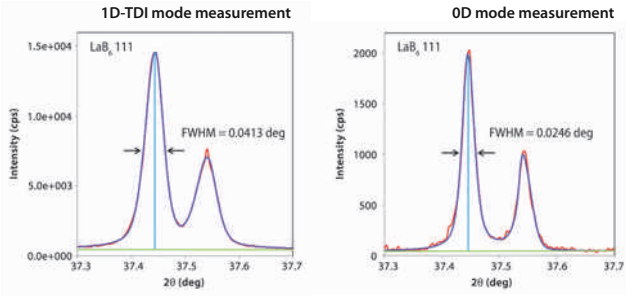

Figure 4. X-ray diffraction pattern of Al_2O_3 powder

Figure 5. X-ray diffraction patterns of LaB_6 powder

Featured Rigaku Journal Article

Integrated X-ray powder diffraction software, "PDXL"

Application software development, Rigaku Corporation

Due to ongoing improvements in X-ray diffractometers, a modern application software package for X-ray powder diffraction supports a wide variety of applications. It includes basic phase identification, of course, but also supports quantification by various methods including, size and strain analysis, whole powder pattern deconvolution (WPPD), Rietveld refinement and structure determination of unknown crystal structures. Rigaku's integrated X-ray powder diffraction software, PDXL, enables one to carry out that series of applications step by step following a user guidance flow bar. In this article, the concepts of the software with application examples are presented.

Click here for full article

Customer in the Spotlight

Advanced Practical at the University of Southampton

The advanced practical is a newly developed program at the University of Southampton, which was implemented from September 2013. As part of this, a 2-day experiment was designed for third year undergraduate students to introduce them to crystallography and gain some practical experience rather than merely theory-based learning on the subject area.

The practical class uses the Rigaku benchtop systems – the MiniFlex 600 and XtaLAB mini – allowing students access to both single crystal and powder X-ray diffraction techniques. These diffractometers are designed with education in mind and, hence, are easier for undergraduates to operate whilst still obtaining quality data, comparable to other instruments.

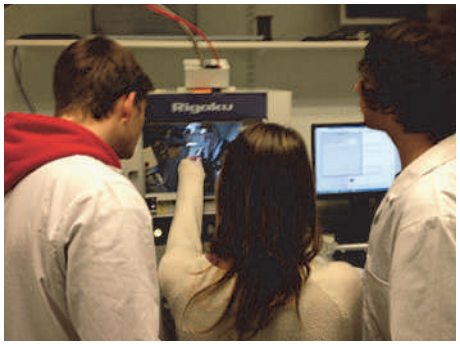

The students' experience was spread over two days of two consecutive weeks to allow a full "start to finish"' procedure to be observed. Initially the students performed a recrystallisation to obtain two different polymorphs and then performed a variety of analytical techniques, including XRPD and SCXRD, to fully characterize and identify the different polymorphs. The diffractometers were driven from online manuals, which allowed the students a more independent experience, being able to operate these themselves, with minimal input from demonstrators.

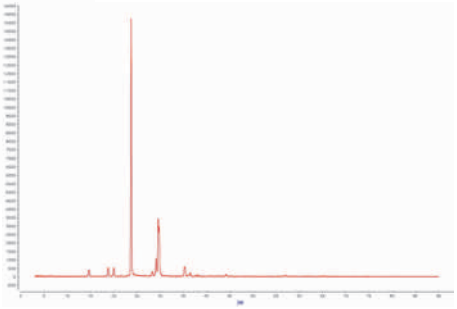

Overall, 70 students carried out the practical over 10 weeks with all successfully completing the experiment, gaining experience and confidence with diffraction techniques and working up the data obtained for full analysis.

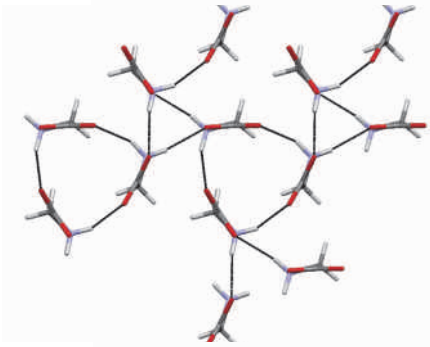

For more information about how the class was organized please contact Dr. Simon Coles, The University of South Hampton, S.J.Coles@soton.ac.uk or Lucy Mapp, L.Mapp@soton.ac.uk

Scientific Book Review

The Perfect Theory. A Century of Geniuses and the Battle over General Relativity
By Pedro G. Ferreira

Hardcover: Houghton Mifflin Harcourt 2014.
ISBN 978-0-547-55489-1

The Perfect Theory is described by the author as a "biography" of Einstein's theory of general relativity. The book is as delightful and entertaining to read as a great mystery novel, the kind that keeps you up until the wee hours or that you have to read twice. The author wants us to intuitively understand why Einstein's theory was and continues to be a revolution in the understanding of gravity and the cosmos. Dr. Ferreira also clearly transmits his great passion for and mastery of science communication in this book.

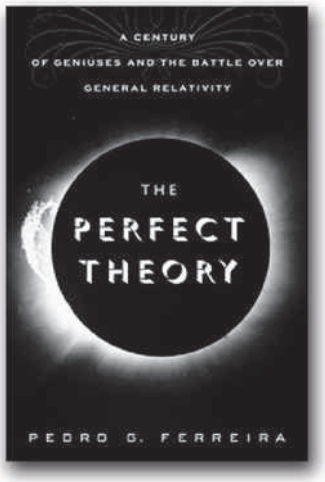

The Perfect Theory is a chronological tale, beginning in the early twentieth century with a description of Albert Einstein's life and the personal and scientific influences on his formulation of general relativity. The story details Arthur Eddington's measurement, during a total eclipse, of the bending of light from distant stars by the sun's gravity. That measurement proved one of the predictions of Einstein's theory and made spacetime a reality.

Subsequent chapters interweave general relativity with major theoretical developments and experimental measurements in gravity and cosmology of the last and current century. Neutron stars, white dwarfs, black holes, quasars, pulsars, singularities, event horizons, and wormholes; all these are characters in the book. The many great geniuses of quantum physics, astrophysics, and cosmology that predicted or measured those phenomena are characterized.

Like a good mystery, every chapter ends with a cliffhanger about how a new great discovery in astronomy, cosmology or astrophysics gave credence to or was inconsistent with general relativity. *The Perfect Theory* made this reader excited to learn about attempts at unification of gravity with other forces and the quantum. On the human side, the author makes clear how the terrible wars and some of the political conflicts of the twentieth century influenced the lives of physicists working on relativity and cosmology.

Time magazine designated Albert Einstein as the "person of the century," the twentieth that is. *The Perfect Theory* will give anyone with a deep curiosity about nature that has heard all the buzzwords like black holes, string theory, M-theory, loop quantum gravity, dark matter and energy, and inflation, an appreciation for the interrelationship of general relativity to all of those. The last few chapters are about the limitations of the theory at extremes of gravity. The book ends on a hopeful note that new technologies and instruments may provide actual experiments that lead to an even more perfect theory of everything.

Laurie Betts, Innatrix, Inc.
Carolina KickStart Labs,
UNC Chapel Hill NC 27599

Conferences

Rigaku exhibited at the AAPG Conference held in Houston, TX, USA, April 6 – 9. The photo above is of two satisfied MiniFlex 600 users with Lori Hatherley of Rigaku. Stephen Kazcmarek (right) is an assistant professor at Bridgewater State University and Brandon Klingensmith (left) is a geologist at FTSI in Houston.

Rigaku will be sponsoring, attending or exhibiting at the following conferences and trade shows:

Biomolecular Structure, Dynamics & Function: Membrane Proteins Mtg
Nashville, TN, USA
May 2

SPIE Defense, Security + Sensing
Baltimore, MD, USA
May 5 – 9

SCSB 18th Structural Bio & Molecular Biophysics Symposium
Galveston, TX, USA
May 17

CPhI South East Asia Jakarta International Expo
Jakarta, Indonesia
May 20 – 22

Click here to see the complete list

Featured EDXRF Application Note

Major oxides in finished cement

X-ray fluorescence (XRF) spectroscopy is a well established technique used in cement plants around the world. The technique is ideal for quality control (QA/QC) throughout the cement production process. Energy dispersive X-ray fluorescence (EDXRF) spectrometry is a routinely employed screening and quality control tool employed to ensure proper composition of incoming feedstocks, raw meal mixture balances, addition of gypsum and throughout the manufacturing process. EDXRF analyzers are also commonly deployed as backup instruments for WDXRF spectrometers used for final QC and certification.

Click here for full application note

Material Analysis in the News

March 29, 2014. Daisy Joseph, Scientific Officer, Nuclear Physics Division, Bhabha Atomic Research Centre (BARC), Mumbai, has underlined the need for in-depth study and use of X-ray fluorescence spectrometry in undergraduate chemistry programs. She noted that the XRF elemental analysis technique has immense potential for wider applications in the spheres of environmental sciences, chemistry, food and product quality monitoring.

April 4, 2014. The Hawaiian Volcano Observatory (HVO) started a cooperative program, with the Geology Department at the University of Hawaii that is designed to share some routine responsibilities related to petrologic monitoring of Kilauea, while training and educating prospective scientists at the same time. Analyses are performed using an XRF instrument at UH-Hilo to detect possible changes in the magma source.

April 4, 2014. Chao Ma and colleagues at the Department of Geoscience, University of Wisconsin - Madison used XRF core scanning to develop a new elemental data set for cyclostratigraphic investigation of Cenomanian/Turonian strata, including the uppermost Lincoln Limestone Member, the Hartland Shale Member, and the Bridge Creek Limestone Member.

April 7, 2014. Minotaur Exploration (ASX: MEP) has completed a single 456 metre diamond drill hole testing the 'Bella Vista' IP anomaly at Catch Dam in South Australia. Geological logging of drill core, supplemented by an XRF instrument, indicated the presence of persistent but low levels of chalcopyrite and sphalerite.

April 12, 2014. Researchers from Penn State University, led by Prof. Tim Murtha, are studing 3,000 years of Mayan cultural evolution in Tikal National Park in Guatemala. They employ XRF spectroscopy to reveal each obsidian artifact's geochemical composition, pinpointing elements like rubidium, iron, copper and zinc so as to determine where obsidian had originally been mined, which made it possible to map out trade networks.

April 14, 2014. UK National Physical Laboratory (NPL) and Loughborough University are setting up a demonstration mobile radiochemistry laboratory that can be driven onto a nuclear site. Instrumentation include a high-resolution gamma spectrometer, a bench-top scintillation detector, portable radon gas detectors and non-nuclear measuring equipment such as balances and X-ray fluorescence, X-ray diffraction, SEM or GC-MS.

April 14, 2014. Work involving a variety of experimental techniques by a group of researchers, led by Thomas H. Epps, III, and Millicent Sullivan in the Department of Chemical and Biomolecular Engineering at the University of Delaware, has shown that routine procedures in handling and processing nanocarrier solutions can have a significant influence on the size and shape of these miniscule structures.

April 20, 2014. Filipino children that are into art are at risk of exposure to toxic heavy chemicals that can damage their brain and development. XRF instrumentation was used to screen samples of watercolor sets from three legitimate school supply stores in the cities of Makati, Manila and Quezon for heavy metals toxins.

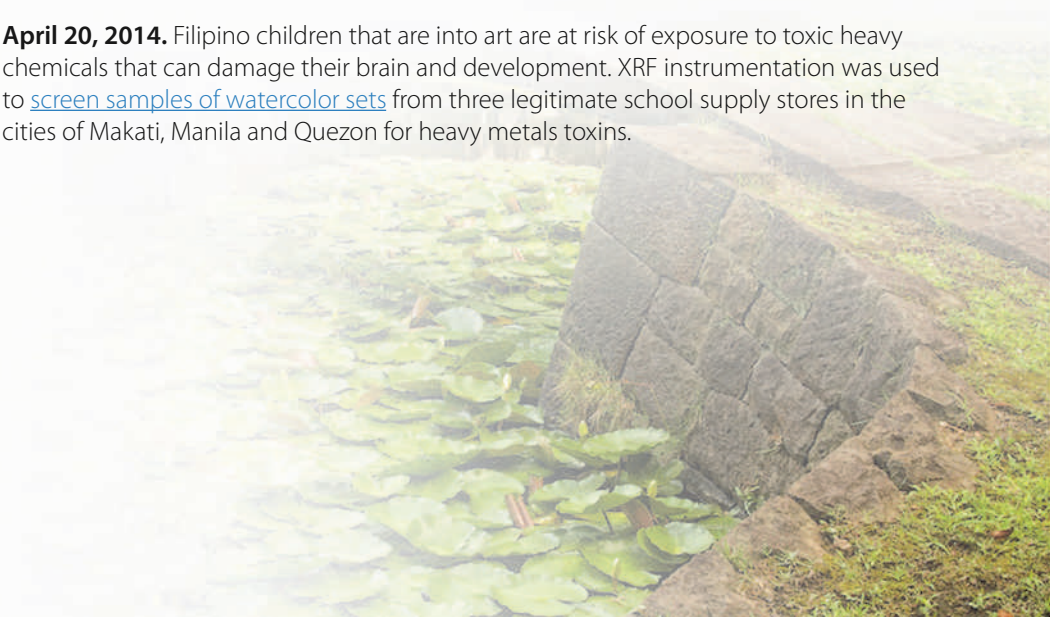

The Adventures of Captain Nano

ISOLATION — Dr. F. Furter forgot to consider how he would return after his failed attemp to intervene in nanoland. He makes a curious discovery.

Recent Scientific Papers of Interest

Diffusion-driven precipitate growth and ripening of oxygen precipitates in boron doped silicon by dynamical X-ray diffraction. Will, J.; Gröschel, A.; Bergmann, C.; Spiecker, E.; Magerl, A. Journal of Applied Physics. 4/15/2014, Vol. 115 Issue 12, p123505-1-123505-8. 8p. 2 Black and White Photographs, 5 Charts, 6 Graphs. DOI: 10.1063/1.4868586.

Temperature, pressure, and size dependence of Pd-H interaction in size selected Pd-Ag and Pd-Cu alloy nanoparticles: *In-situ* X-ray diffraction studies. Sengar, Saurabh K.; Mehta, B. R.; Kulriya, P. K. Journal of Applied Physics. 4/1/2014, Vol. 115 Issue 11, p114308-1-114308-7. 7p. 1 Black and White Photograph, 1 Diagram, 1 Chart, 4 Graphs. DOI: 10.1063/1.4868903.

Structural and Thermodynamics Properties of $TiC_{1-x}N_x$-$TiO_{1-x}N_x$ Solid Solutions: X-ray Diffraction and First-Principles Approaches. Jiang, Bo; Ying, Nantao; Wang, Qiuyu; Xiao, Jiusan; Huang, Kai; Hou, Jungang; Zhu, Hongmin. Journal of the American Ceramic Society. Apr2014, Vol. 97 Issue 4, p1288-1295. 8p. DOI: 10.1111/jace.12761.

Structure of Na_2O–GeO_2–P_2O_5 glasses by X-ray and neutron diffraction. Hoppe, U.; Wyckoff, N.P.; Brow, R.K.; von Zimmermann, M.; Hannon, A.C. Journal of Non-Crystalline Solids. Apr2014, Vol. 390, p59-69. 11p. DOI: 10.1016/j.jnoncrysol.2014.02.013.

Time-resolved X-ray diffraction studies of solidification microstructure evolution in welding. Mirihanage, W.U.; Di Michiel, M.; Reiten, A.; Arnberg, L.; Dong, H.B.; Mathiesen, R.H. Acta Materialia. Apr2014, Vol. 68, p159-168. 10p. DOI: 10.1016/j.actamat.2014.01.040.

Thermal expansion behaviour of a versatile monazite phase with simulated HLW: A high temperature x-ray diffraction study. Asuvathraman, R.; Kutty, K.V. Govindan. Thermochimica Acta. Apr2014, Vol. 581, p54-61. 8p. DOI: 10.1016/j.tca.2014.02.009.

Intrinsic shape analysis of X-ray diffraction using Stokes deconvolution. Ebeid, M.R.; Kaid, M.A.; Ali, M.G.S. Canadian Journal of Physics. Apr2014, Vol. 92 Issue 4, p316-320. 5p. 1 Diagram, 2 Charts, 8 Graphs. DOI: 10.1139/cjp-2013-0134.

Combined high-energy synchrotron X-ray diffraction and computed tomography to characterize constitutive behavior of silica sand. Cil, Mehmet B.; Alshibli, Khalid; Kenesei, Peter; Lienert, Ulrich. Nuclear Instruments & Methods in Physics Research Section B. Apr2014, Vol. 324, p11-16. 6p. DOI: 10.1016/j.nimb.2013.08.043.

Electrodeposition as a Preconcentration and Sample Preparation Technique for Trace Selenium and Tellurium Determination by X-Ray Fluorescence Spectrometry. Li, Qiang; Zheng, Hongtao; Zhu, Zhenli; Tang, Zhiyong. Analytical Letters. Apr2014, Vol. 47 Issue 5, p843-854. 12p. DOI: 10.1080/00032719.2013.853180.

Determination of Trace Elements in Honey from Different Regions in Rio de Janeiro State (Brazil) by Total Reflection X-Ray Fluorescence. Ribeiro, Roberta de Oliveira Resende; Mársico, Eliane Teixeira; Jesus, Edgar Francisco Oliveira; Silva Carneiro, Carla; Júnior, Carlos Adam Conte; Almeida, Eduardo; Filho, Virgílio Franco do Nascimento. Journal of Food Science. Apr2014, Vol. 79 Issue 4, pT738-T742. 5p. DOI: 10.1111/1750-3841.12363.

Application of total reflection X-ray fluorescence spectrometry for multi-elements characterization in human hair. Yadav, V.; Pillay, R.; Jha, S. Journal of Radioanalytical & Nuclear Chemistry. Apr2014, Vol. 300 Issue 1, p57-60. 4p. DOI: 10.1007/s10967-014-2945-0.

Characterization of nuclear materials by total reflection X-ray fluorescence spectrometry. Misra, N. Journal of Radioanalytical & Nuclear Chemistry. Apr2014, Vol. 300 Issue 1, p137-145. 9p. DOI: 10.1007/s10967-014-2972-x.

Interpretation of X-ray diffraction patterns of (nuclear) graphite. Zhou, Z.; Bouwman, W.G.; Schut, H.; Pappas, C. Carbon. Apr2014, Vol. 69, p17-24. 8p. DOI: 10.1016/j.carbon.2013.11.032.

***In situ* monitoring of structural changes during the adsorption on flexible porous coordination polymers by X-ray powder diffraction: Instrumentation and experimental results.** Bon, Volodymyr; Senkovska, Irena; Wallacher, Dirk; Heerwig, Andreas; Klein, Nicole; Zizak, Ivo; Feyerherm, Ralf; Dudzik, Esther; Kaskel, Stefan. Microporous & Mesoporous Materials. Apr2014, Vol. 188, p190-195. 6p. DOI: 10.1016/j.micromeso.2013.12.024.

Non-destructive laboratory-based X-ray diffraction mapping of warpage in Si die embedded in IC packages. Wong, C.S.; Bennett, N.S.; Manessis, D.; Danilewsky, A.; McNally, P.J. Microelectronic Engineering. Apr2014, Vol. 117, p48-56. 9p. DOI: 10.1016/j.mee.2013.12.020.

Studies of kidney stones using INAA, EDXRF and XRD techniques. Srivastava, A.; Swain, K.; Vashisht, B.; Aggarwal, P.; Mete, U.; Acharya, R.; Wagh, D.; Reddy, A. Journal of Radioanalytical & Nuclear Chemistry. Apr2014, Vol. 300 Issue 1, p191-194. 4p. DOI: 10.1007/s10967-014-2939-y.

Cap rock efficiency and fluid circulation of natural hydrothermal systems by means of XRD on clay minerals (Sutri, Northern Latium, Italy). Corrado, Sveva; Aldega, Luca; Celano, Antonio Stefano; De Benedetti, Arnaldo Angelo; Giordano, Guido. Geothermics. Apr2014, Vol. 50, p180-188. 9p. DOI: 10.1016/j.geothermics.2013.09.011.

***In-situ* SAXS study of the plastic deformation behavior of polylactide upon cold-drawing.** Stoclet, G.; Lefebvre, J.M.; Séguéla, R.; Vanmansart, C. Polymer. Apr2014, Vol. 55 Issue 7, p1817-1828. 12p. DOI: 10.1016/j.polymer.2014.02.010.

Relaxation transition in glass-forming polybutadiene as revealed by nuclear resonance X-ray scattering. Kanaya, Toshiji; Inoue, Rintaro; Saito, Makina; Seto, Makoto; Yoda, Yoshitaka. Journal of Chemical Physics. 4/13/2014, Vol. 140 Issue 14, p144906-1-144906-5. 5p. DOI: 10.1063/1.4869541.

Grazing incidence X-ray scattering showing self-organized regular three-dimensional nanopillar-like structures. Paul, Amitesh; Paul, Neelima. Journal of Applied Physics. 4/1/2014, Vol. 115 Issue 11, p114303-1-114303-1. 4p. 3 Graphs. DOI: 10.1063/1.4868690.

Evolution of the heterogeneous structure of model sodium silicate glasses during binodal decomposition: X-ray small-angle scattering investigation. Vasilevskaya, T. Physics of the Solid State. Apr2014, Vol. 56 Issue 4, p771-779. 9p. DOI: 10.1134/S1063783414040350.

***In situ* observation of the orientation relationship at the interface plane between substrate and nucleus using X-ray scattering techniques.** Brown, A.J.; Dong, H.B.; Howes, P.B.; Nicklin, C.L. Scripta Materialia. Apr2014, Vol. 77, p60-63. 4p. DOI: 10.1016/j.scriptamat.2014.01.023.

Real time X-ray scattering study of the formation of ZnS nanoparticles using synchrotron radiation. Rath, T.; Novák, J.; Amenitsch, H.; Pein, A.; Maier, E.; Haas, W.; Hofer, F.; Trimmel, G. Materials Chemistry & Physics. Apr2014, Vol. 144 Issue 3, p310-317. 8p. DOI: 10.1016/j.matchemphys.2013.12.045.

EDXRF Application Note

Major Oxides in Finished Cement

#1273

SCOPE

The analysis of finished Portland cement is demonstrated using the empirical approach.

BACKGROUND

X-ray fluorescence (XRF) spectroscopy is a well established technique used in cement plants around the world. The technique is ideal for quality control (QA/QC) throughout the cement production process. Energy dispersive X-ray fluorescence (EDXRF) spectrometry is a routinely employed screening and quality control tool employed to ensure proper composition of incoming feedstocks, raw meal mixture balances, addition of gypsum and throughout the manufacturing process. EDXRF analyzers are also commonly deployed as backup instruments for WDXRF spectrometers used for final QC and certification.

INSTRUMENTATION

Model:	Rigaku NEX QC$^+$
X-ray tube:	50kV 4W Ag-anode
Detector:	SDD
Sample Type:	Portland Hydraulic Cement
Film:	Prolene
Analysis Time:	200 sec
Environment:	Helium
Standard:	Single position
Optional:	Autosampler

SAMPLE PREPARATION

Each sample is prepared by grinding to a fine, dry, homogeneous powder of <200 mesh (<75um particle size) using a ball mill or ring-and-puck shatterbox. For measurement, a sample is prepared by weighing 5 grams of sample and making a hydraulically pressed pellet using 20 tons pressure for 30 seconds.

Applied Rigaku Technologies, Inc. • 9825 Spectrum Drive, Bldg. 4, Suite 475 • Austin, TX 78717 USA
www.RigakuEDXRF.com • info@RigakuEDXRF.com • (+1) 512-225-1796

CALIBRATION – SINGLE POSITION

Empirical calibrations were built using a set of 8 NIST SRM certified standards: 1880b, 1881a, 1884b, 1885a, 1886a, 1887a, 1888a, 1889a. Using the empirical approach, "alpha corrections" are then employed to automatically compensate for variations in X-ray absorption and enhancement effects within the sample due to the independent variations in element concentration, thus yielding a very accurate model characterizing the cement type.

The single position window ring was used, giving the optimum sensitivity for Na, Mg, Al and Si. The 6-position autosampler can be used for its ease of use, allowing for multiple calibration or unknown samples to be measured without an operator attending the analyzer. Due to a slight difference in sample height, a small change in sensitivity and performance may be seen.

A summary of a typical finished Portland cement empirical calibration is shown here.

Component	Concentration Range (mass%)	RMS Deviation	R^2 Confidence
SiO_2	18.637 – 22.380	0.098	0.9943
Al_2O_3	3.875 – 7.060	0.021	0.9997
Fe_2O_3	0.152 – 3.681	0.013	0.9999
CaO	57.58 – 67.87	0.032	0.9999
MgO	0.814 – 4.740	0.018	0.9998
SO_3	2.086 – 4.622	0.046	0.9972
Na_2O	0.091 – 1.068	0.092	0.9372

REPEATABILITY – SINGLE POSITION

To demonstrate repeatability (precision), NIST SRM 1887a was chosen from the set of calibration standards. The sample was measured in static position for ten repeat analyses using a total analysis time of 200 sec per measurement, with typical results shown below.

NIST SRM 1887a	SiO_2	Al_2O_3	Fe_2O_3	CaO	MgO	SO_3	Na_2O
Standard Value	18.64	6.20	2.86	60.90	2.84	4.62	0.48
Average Value	18.78	6.36	2.81	61.90	2.99	4.65	0.68
Standard Deviation	0.03	0.03	0.01	0.07	0.04	0.02	0.05

Separate calibrations should be used for Raw Meal, Clinker and Finished cement. Performance for Raw Meal and Clinker is comparable to the performance for Finished cement shown here.

Applied Rigaku Technologies, Inc. • 9825 Spectrum Drive, Bldg. 4, Suite 475 • Austin, TX 78717 USA
www.RigakuEDXRF.com • info@RigakuEDXRF.com • (+1) 512-225-1796

TYPICAL DETECTION LIMITS – SINGLE POSITION

To determine the Lower Limit of Detection (LLD) using the empirical method, ten repeat analyses of blank sample were measured and the standard deviation calculated. The LLD is then defined as three times the standard deviation. Actual detection limits may vary based on analysis time used, combinations of elements present and elemental concentration levels. To simulate detection limits in a high calcium matrix, CaO was chosen as the "blank" material.

Component	Lower Limit of Detection
SiO_2	0.01
Al_2O_3	0.02
Fe_2O_3	0.01
MgO	0.11
SO_3	0.05
Na_2O	0.21

REPORTING RESULTS

Analysis results are reported on the main screen and printed. Simply scroll down to see the Lime Saturation Factor, Silicon Ratio and Aluminum Ratio.

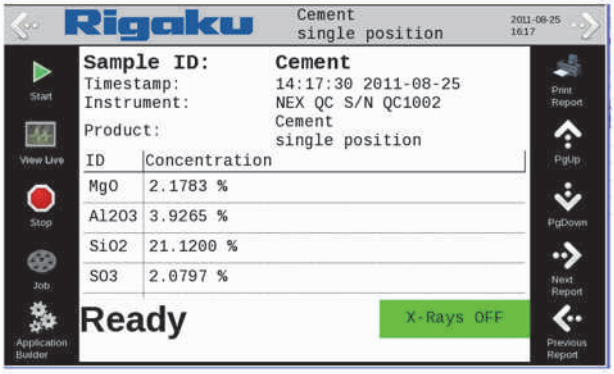

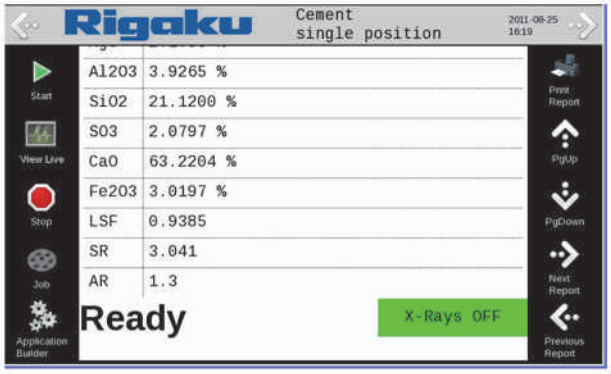

Standard formulas for LSF, SR and AR are used.

LSF Finished = (CaO – 0.7SO3)/(2.8SiO2 + 1.2Al2O3 + 0.65Fe2O3)

Clinker SLF = CaO/(2.8SiO2 + 1.2Al2O3 + 0.65Fe2O3)

SR = SiO2/(Al2O3 + Fe2O3)

AR = Al2O3/Fe2O3

CONCLUSION

During the entire production and processing cycle, oxide composition of the cement material must be reliably monitored to ensure optimal process control, physical characteristics of the cement, as well as profitability. The Rigaku NEX QC$^+$ gives the cement plant a reliable and rugged low-cost system for quality control measurements around the plant, making it an ideal tool throughout the quality control process and as a backup to WDXRF systems. Similar performance as shown here is also applicable to clinker and raw meal materials, and can be used simply to measure gypsum (SO3) in finished cement.

Applied Rigaku Technologies, Inc. • 9825 Spectrum Drive, Bldg. 4, Suite 475 • Austin, TX 78717 USA
www.RigakuEDXRF.com • info@RigakuEDXRF.com • (+1) 512-225-1796

Smart Sample Loading System

Smart Sample Loading System

Rigaku's new Smart Sample Loading System (SSLS) adds a new dimension of flexibility to the ZSX Primus WDXRF spectrometer. For sample types that are amenable to such a process, a vacuum chuck can be used to load samples into pre-loaded sample holders. This sample loading system has two important consequences: time is saved by the operator since they are no longer required to manually load each sample in a sample cup and the number of samples that can be held on the sample deck is increased significantly.

The Smart Sample Loading System is an optional configuration for the ZSX Primus spectrometer

The sample deck can be configured to handle different sample sizes

Permissible sample types

Rigaku's SSLS can handle samples up to 50 grams in weight and the modular sample deck racks have been designed for different sample diameters. Samples with a diameter of 35 mm can be stored 32 samples to a rack with three such racks sitting on the deck. Samples with a diameter of 40 mm can be stored 24 samples to a rack with a possibility of three of these racks on the deck. In addition, the racks can be mixed so that different sample sizes are easily accommodated on the deck at the same time.

Sample types that are amenable to this type of loading procedure include fused glass beads and pressed powders. Both plastic and metal pressed powder holders are permitted.

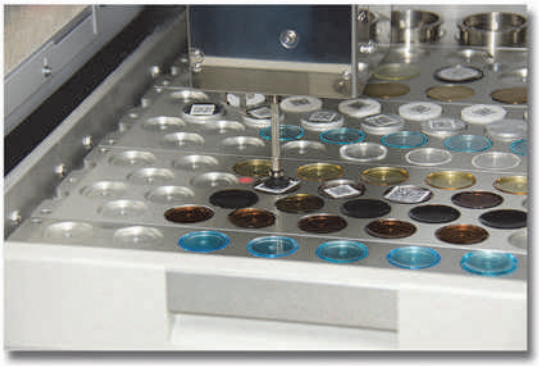

Vacuum chuck retrieving sample from deck

Sample handling

A precision vacuum chuck is used to safely and reproducibly pick up the samples and place them in the measurement sample holder. Each sample type has a specific sizing ring positioned in the measurement sample holders to assure that the sample is properly positioned for measurement, and the analytical reading surface is never compromised.

Improve sample handling efficiency and throughput

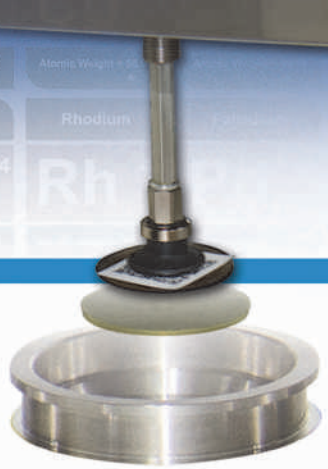

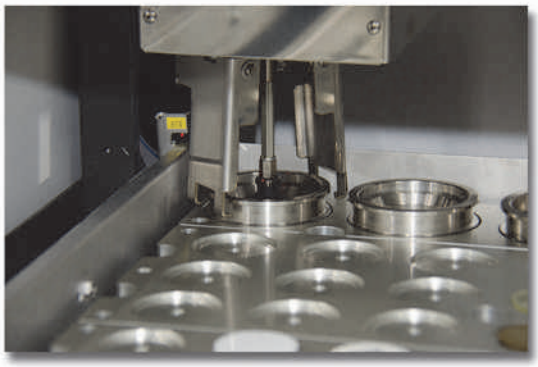

The first two samples are loaded into sample holders stored on the deck

Sample loading protocol

The first two samples are loaded into sample holders that are stored at the back of the deck. Once the sample holders are inserted into the instrument, they remain and after measurement the holderless sample is returned to its position on the deck. Samples three and on are picked up and loaded directly into the sample holder that is already in the pre-evacuation chamber.

A two-dimensional barcode can be affixed to the non-analysis of the sample

Sample tracking

Keeping track of samples has never been easier. A two-dimensional barcode can be attached to the non-analysis surface of each sample. Before the sample is lowered into the pre-evacuation chamber through the input port, the barcode is scanned and the sample information is loaded into the control software.

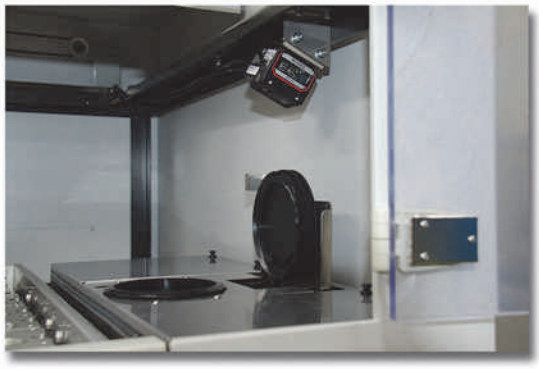

The barcode reader is positioned above the pre-evacuation chamber

Improve efficiency and throughput

Rigaku's new SSLS is an easy way to improve efficiency and throughput. Operators will spend less time loading sample holders and greatly increase the capacity of the deck, allowing for longer uninterrupted operation.

Integrated X-ray powder diffraction software

PDXL

—For more advanced analysis—

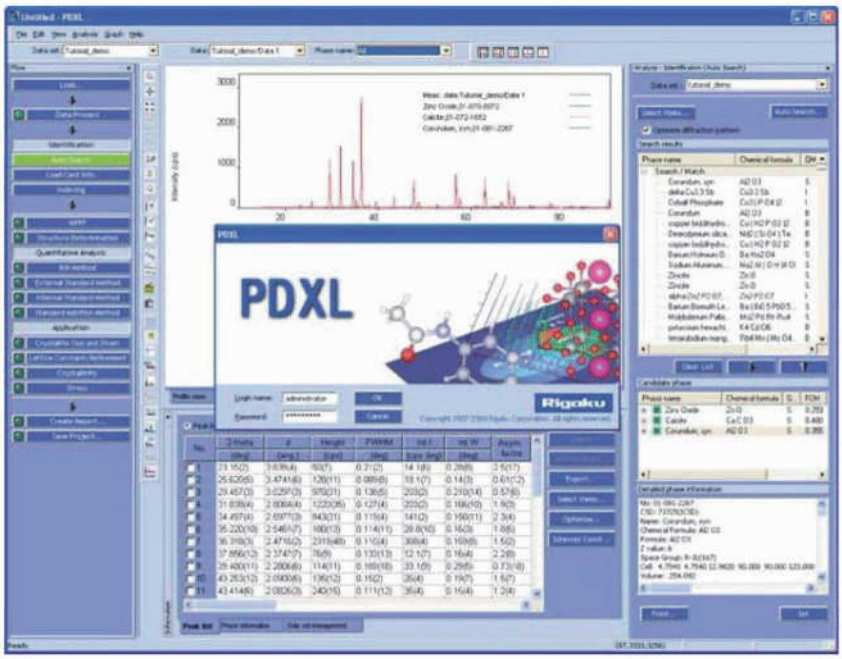

1. Introduction

X-ray powder diffraction (XPD) analysis has been widely used in the field of materials science, such as materials development or quality control for over fifty years. However, many scientists and engineers may not be aware of exactly how much information XPD can provide on a sample. Using previous generations of software, high degrees of background knowledge and practical experience have been required to successfully obtain useful analysis results.

In the last five years, both diffractometer and data-analysis software have made significantly advances. New developments of high-speed position sensitive detectors make possible a rapid collection of high-resolution and high-intensity diffraction data. Improvements in PC processing speed make easy the use of an entire experimental pattern, known as "whole-pattern analysis", for a rapid and precise structure analysis of a material. The whole-pattern analysis method is becoming more popular than the conventional analysis methods, which use only certain diffraction peaks to obtain information on specific topics of materials science.

Ab-initio crystal-structure analysis of unknown samples is also gaining popularity in XPD analysis. Many users used to consider this type of XRD analysis difficult because 3-dimensional diffraction data is "flattened" into one- or two-dimensions. There is a misconception that whole-pattern analysis, such as the Rietveld analysis or *ab-initio* crystal structure analysis, is difficult to perform and requires advanced know-how and technical understanding. With this in mind, Rigaku Corporation has developed PDXL, a new application software package created to enable the user who is not familiar with whole pattern analysis to easily perform Rietveld or *ab-initio* crystal-structure analysis with just a few clicks.

Many kinds of information can be obtained from XPD data. PDXL allows the user to perform many types of analysis using a single platform, making it possible to obtain a diverse array of analysis results from one single XPD pattern. The following sections describe how to use PDXL, and several new features in PDXL are also introduced.

2. Analysis

2.1. Automatic peak processing

Most XPD data analysis is performed based on

Fig. 1. Peak list created immediately after loading data.

diffraction-peak information such as peak position, intensity, width, etc. The user used to have to perform several separate data processing steps, including smoothing, background subtraction and peak decomposition, to obtain accurate values for peak position, intensity, and width. PDXL automatically carries out smoothing, background subtraction and peak decomposition, and even creates a peak list as soon as measurement data is loaded (Fig. 1). No user intervention is needed, making PDXL's results free from human error.

2.2. Phase identification

Phase identification is one of the most common objectives of XPD data analysis. Using the PDXL's proprietary Hybrid Search/Match algorithm, crystalline phases (or compounds) presented in a sample can be identified by searching a reference database such as the ICDD's PDF-2.[1] This algorithm checks the degree of coincidence between experimentally measured data and the entries in the reference database, as well as crystallographic data registered in the database with modified lattice constants and preferred orientation within a specified tolerance. Therefore, the Hybrid Search/Match algorithm provides accurate results for the phase identifications of mixtures including solid-solution and highly-oriented samples (see Fig. 2).

The Hybrid Search/Match algorithm consecutively identifies one phase after another in a sample. After identifying the first phase, the peak intensities of the identified phase are subtracted from the experimental pattern. Then the algorithm will look for a second phase in the residual peaks. After the second phase is identified, the peak intensities of the identified phase will again be subtracted from the residual peaks. This procedure will be repeated until no new possible phases can be identified (Figs. 3a–d).

An automatic search for major and minor compounds can be initiated by just clicking the *Execute search*

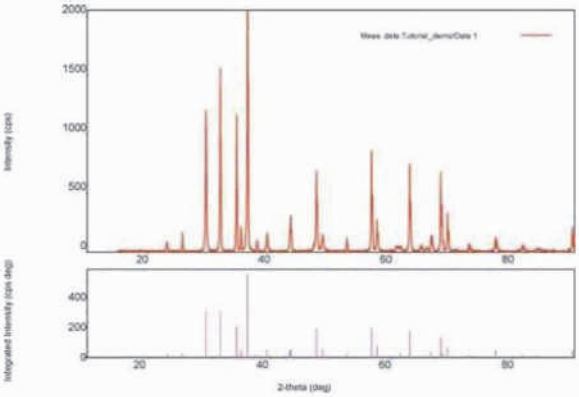

Fig. 3(a). Experimental XRD pattern (top) and integrated intensities (bottom).

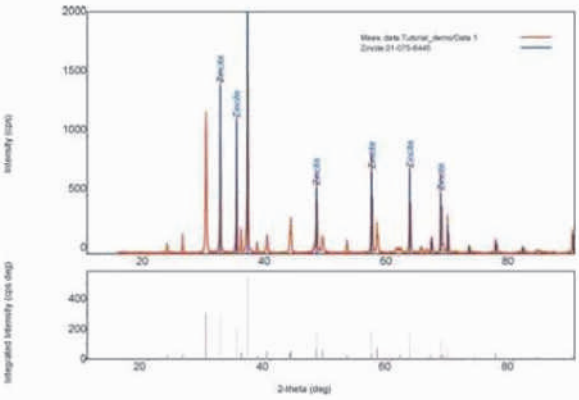

Fig. 3(b). Residual peaks after identifying zincite (see purple bars in the bottom graph).

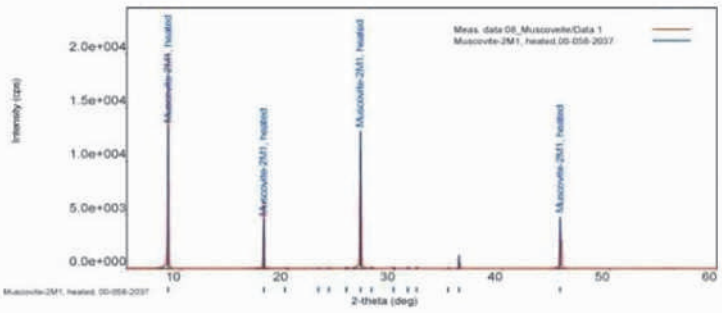

Fig. 2. Identification of a highly-oriented muscovite sample.

[1] See http://www.icdd.com/products/pdf2.htm.

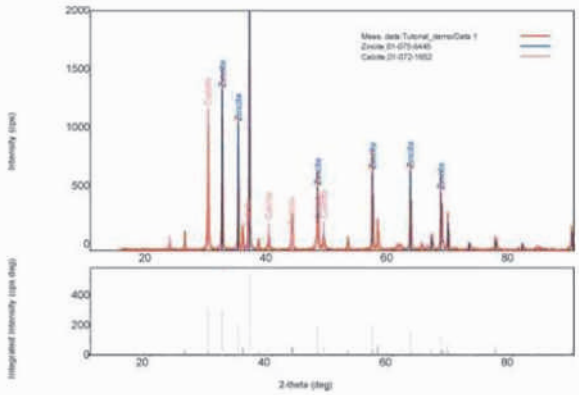

Fig. 3(c). Residual peaks after identifying calcite.

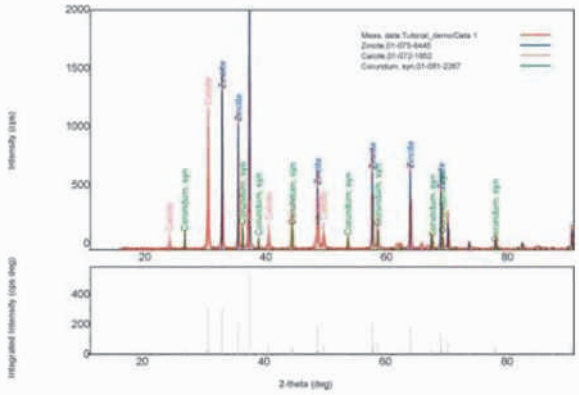

Fig. 3(d). Residual peaks after identifying corundum (most peaks disappear from the bottom graph).

Candidate phase

Phase name	Chemical formula	QM	FOM
Zincite	Zn O	S	0.340
Calcite	Ca C O3	S	0.480
Corundum, syn	Al2 O3	S	0.355

Fig. 4. Determined candidate phases.

button. PDXL will also determine a list of crystalline phase candidates after the search is done (Fig. 4).

2.3. Rietveld analysis

Many consider Rietveld analysis to be a difficult task. PDXL has been designed from the ground up to allow even the novice user to easily perform Rietveld analysis. The application of Rietveld analysis extends beyond crystal-structure refinement; Rietveld analysis also provides the user with accurate lattice constants and quantitative values for the identified phases.

After phase identification, Rietveld analysis requires information on the crystal-structure parameters of each phase. Crystal structure parameters can be obtained in several ways. The easiest method is to obtain the information from the corresponding CIF (crystal information file). If ICSD (Inorganic Crystal Structure Database[2]) has been installed on the user's PC, crystal-structure parameters will be automatically loaded when phase identification is complete. After checking the crystal-structure parameters, click the Refine button to start the Rietveld analysis. Previous analysis packages required a user to input the initial values of the lattice constants, peak-profile parameters, background function, preferred orientation parameters, etc. before starting the refinement. PDXL automatically estimates the initial values of these parameters prior to performing the Rietveld refinement (Fig. 5).

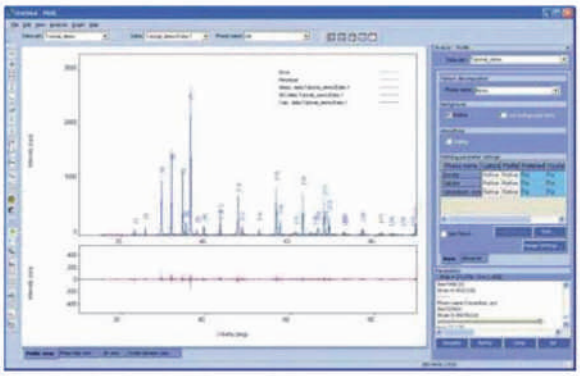

Fig. 5. PDXL main window for Rietveld analysis.

2.4. Analysis-results report

As described above, a lot of information on a sample can be obtained from the analysis of just one XPD pattern. All PDXL results can be viewed in the Analysis Results window (Fig. 6).

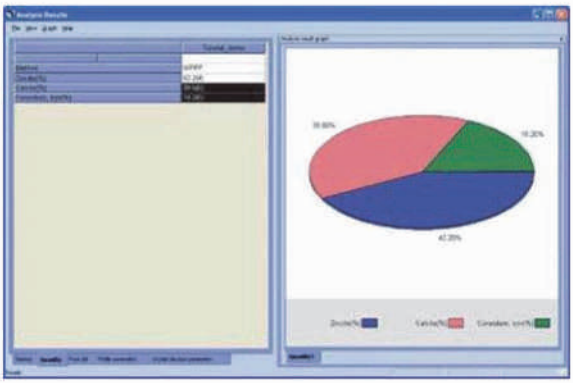

Fig. 6. Analysis Results window.

The user can create graphs of the results, including lattice constants, quantitative XRD analysis, etc. The values obtained from a single analysis can be indicated in a pie chart. PDXL can also generate bar charts to compare results obtained from several XRD patterns.

PDXL makes use of the macro features of Microsoft Word® to create analysis-result reports. PDXL has

[2] See http://www.jaici.or.jp/wcas/wcas_icsd.htm.

several templates for creating reports, which can be used to automatically generate analysis-result reports that are ready for publication (Fig. 7). The template files can also be customized.

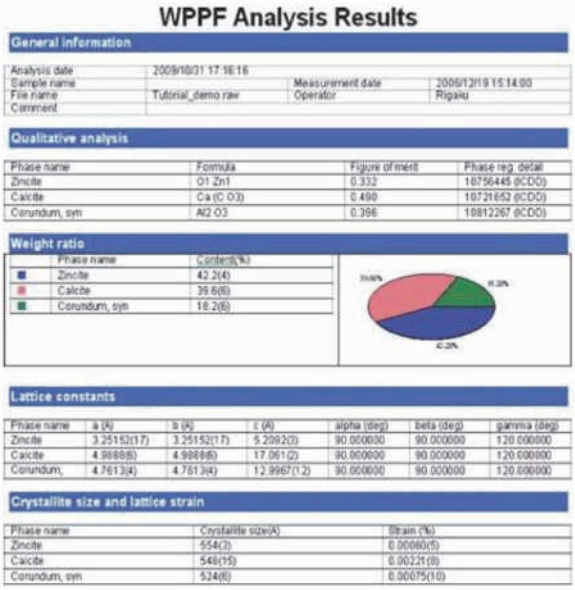

WPPF Analysis Results

General information

Analysis date	2009/10/31 17:16:16		
Sample name		Measurement date	2005/12/19 15:14:00
File name	Tutorial_demo.raw	Operator	Rigaku
Comment			

Qualitative analysis

Phase name	Formula	Figure of merit	Phase reg. detail
Zincite	O1 Zn1	0.332	16756445 (ICDD)
Calcite	Ca (C O3)	0.490	10721652 (ICDD)
Corundum, syn	Al2 O3	0.396	10812267 (ICDD)

Weight ratio

Phase name	Content(%)
Zincite	42.2(4)
Calcite	39.6(6)
Corundum, syn	18.2(6)

Lattice constants

Phase name	a (A)	b (A)	c (A)	alpha (deg)	beta (deg)	gamma (deg)
Zincite	3.25152(17)	3.25152(17)	5.2092(3)	90.000000	90.000000	120.000000
Calcite	4.9888(6)	4.9888(6)	17.061(2)	90.000000	90.000000	120.000000
Corundum,	4.7613(4)	4.7613(4)	12.9967(12)	90.000000	90.000000	120.000000

Crystallite size and lattice strain

Phase name	Crystallite size(A)	Strain (%)
Zincite	554(2)	0.00060(5)
Calcite	548(15)	0.0022f(8)
Corundum, syn	524(6)	0.00075(10)

Fig. 7. Sample analysis-result report.

2.5. Automation

During the research and development of a new material, it is often necessary to compare the qualitative and quantitative analysis results of related samples synthesized under different conditions. To compare the results of one sample with those of other samples, all experimental datasets need to be analyzed under the same analysis conditions. The automation feature in PDXL makes it easy for the user to do so. Automation applies a predefined analysis process to several different measured datasets, from the initial data processing to report creation. After the setting and saving analysis conditions for one of the measured datasets, the saved conditions can be automatically applied to the analysis of all remaining datasets consecutively (Fig. 8). Therefore, the user only has to select which datasets are to be loaded and analyzed. When the data analysis is complete, all results will be displayed on the screen in an easy-to-compare format (Fig. 9).

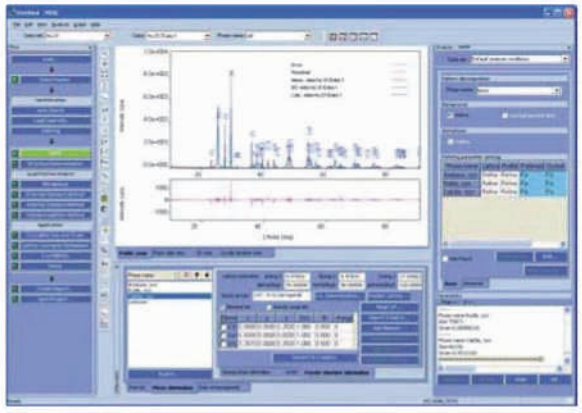

Fig. 8. Setting conditions for automation.

Fig. 9. Comparison of the results of ten samples.

2.6. Quantitative analysis

For quantitative XRD analysis, PDXL uses a well-known conventional "calibration" method, which uses one or more diffraction peaks instead of the entire diffraction pattern. With the calibration method, standard reference samples are used to obtain an accurate quantitative analysis of a sample. Once calibration plots have been created they can be applied to any measured data obtained under the same conditions, as many times as required. PDXL can save the calibration data in the PDXL project format for future use. Similarly, PDXL can save calibration data in the PDXL project format to make corrections to peak positions for lattice constant refinement, peak widths for crystallite size analysis, etc.

3. *Ab-initio* crystal structure analysis

As described above, conventional XPD data is missing certain diffraction-peak information because the three-dimensional XPD data is compressed into one dimension. Therefore, it has traditionally been considered difficult to solve crystal structures using the direct method, which requires a large number of diffraction peaks.

However, the direct space method, which makes use of global optimizations such as the simulated annealing method, has recently been gaining popularity owing to significant improvements in the performance of computers. The direct space method places a molecular-structure model in a unit cell and optimizes the gravity center and Euler angles of the molecule to determine the crystal structure of a compound. The most commonly used method for crystal-structure analysis using XPD data has been to refine the atomic coordinates of another analogous crystal structure by the Rietveld method. On the other hand, the *ab-initio* crystal-structure analysis of a sample with an unknown crystal structure is performed in the same way that a single-crystal structure is determined. Rigaku Corporation has developed a crystal-structure analysis package for PDXL which includes direct method using EXPO2009 [Altomare et

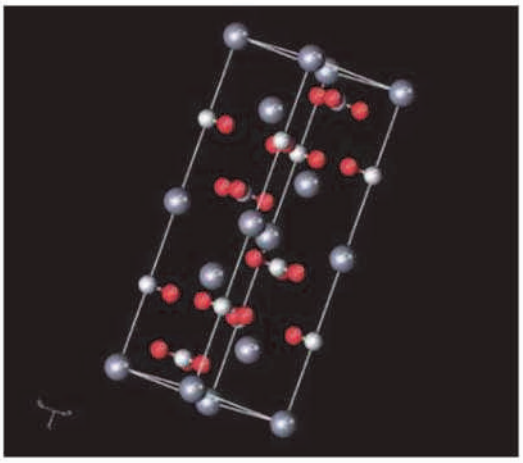

Fig. 10. Crystal structure of calcite, $CaCO_3$.

al., *J. Appl. Cryst.*, **42** (2009), 1197–1202], direct space method and charge flipping method functionality. The structure-analysis package is designed to be easy-to-use, simplifying everything from lattice constant determination by automatic indexing to crystal-structure refinement using the Rietveld method. The crystal structure of a compound determined by PDXL can also be viewed three dimensionally on the user's computer. As an example, the three-dimensional crystal structure of calcite, $CaCO_3$, is plotted in Fig. 10. We believe that PDXL makes crystal-structure analysis more accessible to our users.

4. Conclusions

PDXL has been developed as a comprehensive software package for the analysis of XPD data. The number of scientists and engineers using XPD for materials characterization is growing rapidly, and PDXL makes it possible for those who are not specialists in the field of X-ray diffraction to easily perform Rietveld analysis and *ab-initio* crystal-structure analysis. Many different kinds of information and analysis results can be obtained from XPD data. It is our hope at Rigaku that PDXL will help our users to rapidly obtain useful results, and that these results will be instrumental to advances in a wide variety of scientific fields.

Rigaku

X-ray Diffraction Analysis for Thin Film Samples

Training Textbook

Click below to see previously published sections

Chapter 3
Diffraction Measurements

Diffraction measurements are classified by measurement techniques. Measurement techniques vary in the relative positions of the incident X-ray beam, sample crystal, and counter; scanning directions of the axes; and optical resolution. However, all techniques are similar in measuring the change in scattering intensity while rotating the axes.

This chapter uses the concept of the reciprocal lattice introduced in Chapter 2 to discuss the relationship between measurement techniques and what information they can provide on crystal structures and crystallinity. This chapter also describes practical measurement procedures and precautions.

3.1 Relationship between Various Measurement Techniques

The suitable measurement technique can provide a wide range of crystallographic information, including crystal structures, crystallinity, crystal orientation, and lattice constants. As discussed in Section 4.3, changes in these parameters appear in different directions in reciprocal space. As discussed in Section 4.4, we can measure the distribution of scattering intensity in reciprocal space by rotating the axes of the goniometer. By rotating the axes in the direction corresponding to the change in the parameter to be measured, we can obtain the information needed. Diffraction measurement techniques can be classified as shown in Table 3.1.1 based on the scanning method of the axes.

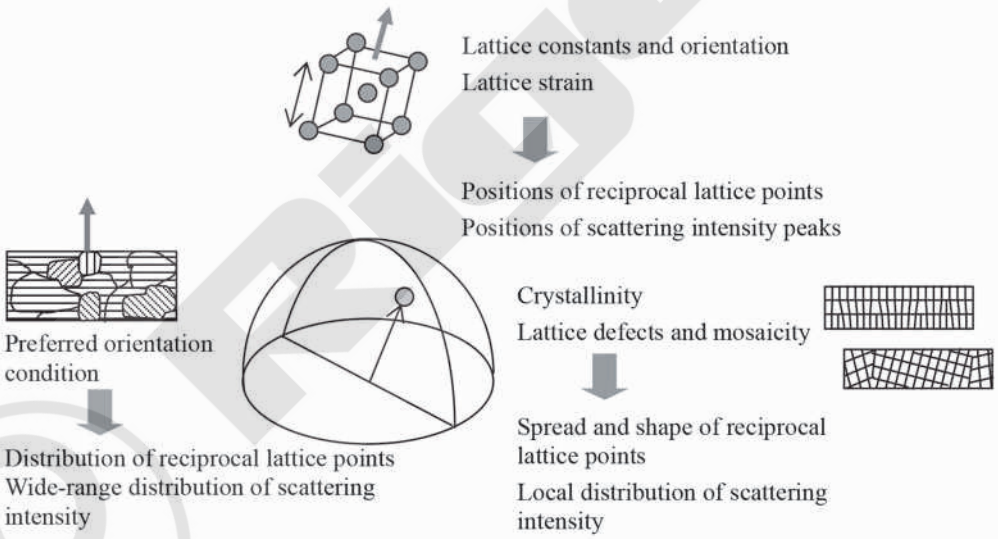

Figure 3.1.1. Relationship between measurement parameters and techniques (Schematic illustration)

Table 3.1.1. Various measurement techniques

Measurement technique	Information obtained	Scan axis
Out-of-plane measurement (One-dimensional scan)	Information on lattice planes parallel to sample surface → Qualitative analysis and crystal structure	$2\theta/\omega$ (Always $2\theta = 2 \times \omega$)
Thin film measurement (One-dimensional scan)	Information near sample surface (applies only to unoriented samples) → Qualitative analysis and crystal structure	2θ (Incident angle, ω, is fixed near the critical angle)
In-plane measurement (One-dimensional scan)	Information on lattice planes near and parallel to sample surface → Qualitative analysis and crystal structure	$2\theta\ \chi/\phi$ (2θ or sum of 2θ and $2\theta\chi$ is fixed at the diffraction angle)
Pole figure measurement (Two-dimensional scan)	Information on distribution of specific crystal orientation → Orientation analysis	$\chi\ (\alpha)$, $\phi\ (\beta)$ (Incident angle, ω, is fixed near the critical angle)
Preferred orientation and crystallinity measurement* (One-dimensional scan)	Information on degree of preferred orientation or crystallinity → Orientation and crystallinity analysis	ω, χ, or ϕ
Rocking curve measurement* (One-dimensional scan)	Information on film structure and crystallinity of epitaxial or single crystal → Crystallinity, film thickness, and composition ratio	$2\theta/\omega$
RSM measurement (Two-dimensional or three-dimensional scan)	Information on d-value of three-dimensional components of preferred orientation, crystal orientation, and degree of preferred orientation → Qualitative analysis, orientation analysis, and crystallinity analysis → Information on film structure and crystallinity of epitaxial or single crystal → Crystallinity analysis and epitaxial analysis	$2\theta/\omega$, ω ($,\chi$ or ϕ) $2\theta/\chi/\phi$, ϕ ($,\chi$ or ϕ)

** For polycrystal measurements, the ω scan for measuring the degree of preferred orientation is sometimes called "rocking curve measurement." To avoid confusion, the term, "rocking curve measurement" will refer specifically to $2\theta/\omega$ scans for an epitaxial or single crystal. The ω scan for measuring the degree of orientation is called "orientation measurement."*

The following sections discuss measurement procedures and measurement data interpretation for the measurement techniques listed in Table 3.1.1.

3.2 What Does Diffraction Measurement Observe?

3.2.1 Out-of-Plane Measurement

Out-of-plane measurement measures diffraction by lattice planes parallel to the sample surface. As Fig. 3.2.1 shows, the incident angle and the exit angle of the X-rays with respect to the sample surface are always equal when you measure diffraction by lattice planes parallel to the sample surface. Such measurements essentially scan the $2\theta/\omega$ axis while maintaining a relationship in which the diffraction angle 2θ is twice the incident angle ω.

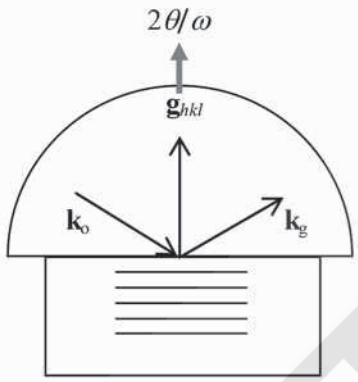

Figure 3.2.1. Schematic illustration of out-of-plane measurement

For example, in the case of a single crystal sample with a surface parallel to the (001) plane, out-of-plane measurement observes the lattice planes parallel to the (001) plane but with different interplanar spacings, such as the (002) and (003) planes. For an oriented polycrystal sample having a fiber orientation such that the (001) plane is parallel to the surface, this technique similarly observes planes parallel to the (001) plane but with different interplanar spacings, such as the (002) and (003) planes. For random polycrystal samples, this technique observes all lattice planes, although the diffraction spots observed here are diffracted from crystallites with lattice planes parallel to the surface.

Thus, out-of-plane measurements can be used for qualitative analysis and for determining the presence or absence of a preferred orientation, interplanar spacings of the lattice planes parallel to the surface, lattice constants corresponding to these interplanar spacings, and the crystallinity of a crystal lattice parallel to the surface. However, out-of-plane measurements cannot observe lattice planes perpendicular to the surface and cannot provide information on the presence or absence of the in-plane orientation. It cannot distinguish between a fiber-oriented and a single crystal sample. To evaluate in-plane orientation, we use asymmetric reflection or in-plane measurement.

3.2.2 Thin Film Measurement

Thin film measurement is an efficient technique for measuring scattering from the region near the surface while avoiding scattering from the substrate. It uses X-ray incidence at a grazing angle relative to the sample surface, changing only the scattering angle during measurement. Here, the incident angle is set near the critical angle at which the X-ray depth of penetration into the sample is extremely low. We can also investigate the depth dependence of sample states using several types of thin film measurement performed while changing the incident angle.

This measurement technique is equivalent to scanning just the scattering angle 2θ while maintaining the incident angle ω at a small angle. Here, as Fig. 3.2.2 shows, as scattering angle 2θ changes, the orientation of the crystal observed changes. Thin film measurement observes lattice planes oriented in all directions with respect to the sample surface. With a single crystal or an oriented sample, this technique observes just the lattice planes corresponding to the reciprocal lattice points that incidentally enter the trajectory of the 2θ scan, as indicated in Fig. 3.2.2.

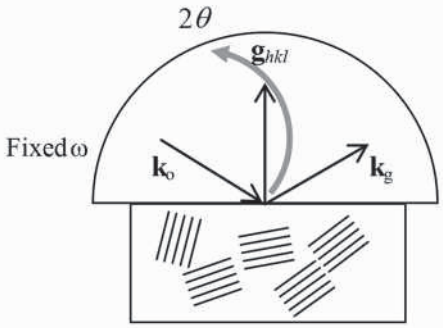

Figure 3.2.2. Schematic illustration of thin film measurement

Thin film measurement can be used for qualitative analysis of an unoriented (or weakly oriented) polycrystal sample and to investigate lattice constants and the crystallinity of such a sample. We can also investigate the depth dependence of these physical quantities. However, this method generally cannot be used to analyze a strongly oriented polycrystal sample or a single crystal sample, since these samples with this technique generate no or virtually no diffraction peaks.

3.2.3 In-Plane Measurement

In-plane measurement measures lattice planes perpendicular to the sample surface. Like thin film measurement, in-plane measurement relies on X-ray incidence at a grazing angle relative to the sample surface. It can acquire information on crystal states in the direction of depth by performing two or more sets of measurements with different incident angles.

If the X-ray beam is incident on the sample at a grazing angle, the total reflection phenomenon will occur if the incident angle is less than the critical angle, in which case X-rays incident on the sample propagate parallel to the sample surface.

When X-rays propagating parallel to the sample surface are diffracted by lattice planes perpendicular to the sample surface, the diffracted X-rays also exit the surface at a grazing angle. Measuring this diffraction is equivalent to scanning the $2\theta\chi/\phi$ axis while maintaining a relationship in which the diffraction angle $2\theta\chi$ perpendicular to the sample surface is twice the sample in-plane rotation angle ϕ. Fig. 3.2.3 shows the direction of the scan in reciprocal space.

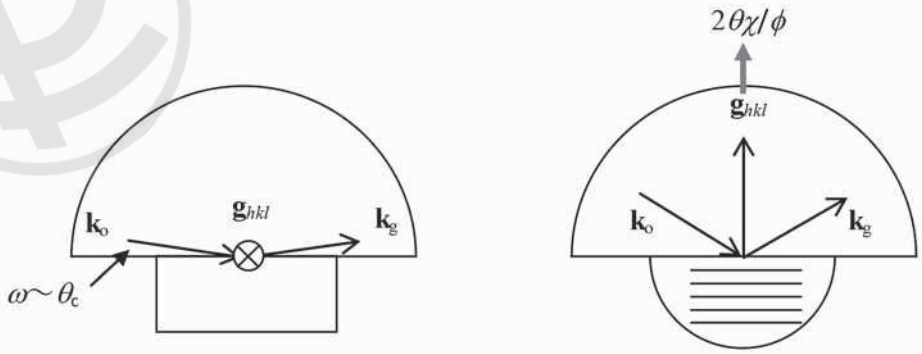

Sample side view *Sample top view*

Figure 3.2.3. Schematic illustration of in-plane measurement

3.2 What Does Diffraction Measurement Observe?

Consider a cubic crystal sample. Assume a single crystal sample with surface parallel to the (001) plane and perpendicular to the (110) plane and a (110) plane in the direction indicated as $2\theta\chi/\phi$ in the top view of Fig. 3.2.3. In this case, the $2\theta\chi/\phi$ scan observes planes parallel to the (110) plane but with different interplanar spacings, such as the (220) and (330) planes. For an oriented polycrystal sample having a fiber orientation such that the (001) plane is parallel to the surface, this technique observes all planes perpendicular to the (001) plane, such as the (100) and (120) planes, in addition to planes parallel to the (110) plane but with different interplanar spacings, such as the (220) and (330) planes. For a random polycrystal sample, this technique observes all lattice planes, although the diffraction spots observed here are diffracted from crystallites having lattice planes perpendicular to the surface.

Thus, in-plane measurement can be used for qualitative analysis and for investigating the presence or absence of the preferred orientation, the interplanar spacings of the lattice planes perpendicular to the surface, lattice constants corresponding to these interplanar spacings, and the crystallinity of the crystal lattice perpendicular to the surface. In addition, since in-plane measurement can observe lattice planes perpendicular to the surface, it can provide information on the presence or absence of in-plane orientation. For example, it can distinguish between a fiber-oriented sample and a single crystal sample or confirm the presence or absence of twinning.

As described above, in-plane measurement can change the depth of analysis by varying the incident angle. The figure below shows the relationship between the incident angle and depth of penetration (the depth at which the incident X-ray intensity drops to 1/e).

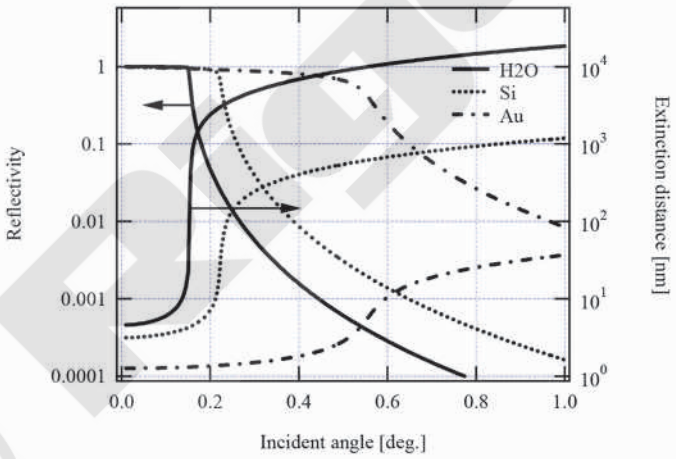

Figure 3.2.4. Incident angle and depth of penetration

As implied by Fig. 3.2.4, the depth of penetration changes abruptly near the critical angle. We can investigate changes in crystal structure or crystallinity in the direction of depth by performing in-plane diffraction measurements while varying the incident angle across the critical angle. We can also identify deposits at the surface or interfaces by qualitatively analyzing two or more measurement results with different incident angles.

3.2.4 Pole Figure Measurement

Pole figure measurement measures diffraction intensity distributions by rotating the sample in all directions while keeping the diffraction angle constant. The direction at which high diffraction intensity is observed corresponds to the preferred direction of the pole figure axes (indicating that crystallites with the measurement planes oriented in that direction are dominant). The pole figure measurement expresses the preferred orientation of the sample with pole figure axes α and β. As shown in Fig. 3.2.5, α and β correspond to the χ and ϕ axes of the four-circle goniometer, respectively.

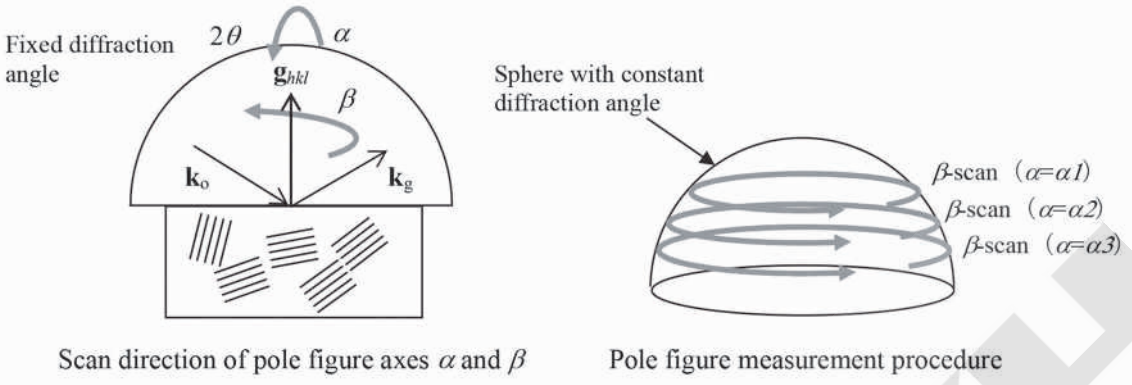

Figure 3.2.5. Schematic illustration of pole figure measurement

The results of pole figure measurement are expressed as a **pole figure** (Fig. 3.2.6).

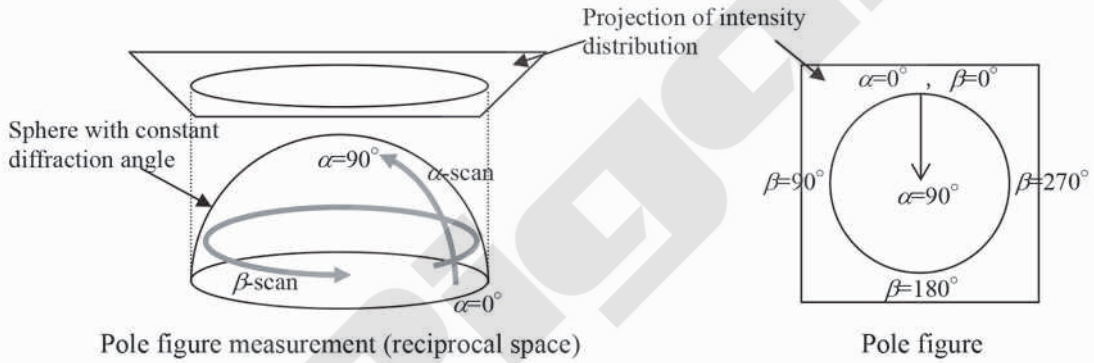

Figure 3.2.6. Pole figure

Consider the example of a cubic crystal sample. Fig. 3.2.7 shows the results of a pole figure measurement of the (111) plane and of the (220) plane perpendicular for three cases: 1. a randomly oriented sample; 2. a sample with the (111) plane fiber-oriented parallel to the surface; and 3. a single crystal sample with the (111) plane parallel to the surface.

For a randomly oriented sample with no preferred orientation as indicated in 1, the pole figures show only a small change in the diffraction intensity in different orientations, producing a flat intensity distribution. The slight orientation dependence of the diffraction intensity is not caused by preferred orientation, but by the change in the area of X-ray irradiation and in absorption accompanied by changes in X-ray incidence and exit angles relative to the surface.

For a sample having the {111} fiber orientation shown in 2, the pole figure of the (111) surface shows strong diffraction intensity at the center (at the point corresponding to the component parallel to the sample surface). This high intensity indicates the dominance of the components satisfying the diffraction condition in this direction—that is, the dominance of crystallites with (111) plane parallel to the surface. For a cubic crystal sample, the {111} planes ((-111), (11-1), and (1-11) planes) are found oriented 70.5° to the (111) plane. All these planes have the same diffraction angle. The pole figure also shows strong diffraction intensity in the direction at α = 70.5°. However, since it lacks an in-plane (β direction) orientation, the pole figure does not have a distribution and shows a ring-shaped intensity distribution. The pole figure of the (220) plane shows the diffraction intensity distribution produced by the {220} planes at 35.3°and 90.0° to the (111) plane.

3.2 What Does Diffraction Measurement Observe?

For a single crystal sample with the (111) plane parallel to the surface of 3, the pole figure of the (111) surface shows strong diffraction intensity at the center and at 70.5° form the (-111); (11-1); and (1-11) planes. Here, the intensity distribution in the β direction does not form a ring-shaped distribution. We observe strong intensity only in the directions in which the {111} planes exist in the single crystal, resulting in the pole figure shown in 3. of Fig. 3.2.7. The pole figure for the (220) plane shows the diffraction intensity distribution produced by the {220} planes found oriented at 35.3° and 90.0° to the (111) plane, as shown in 3. of Fig. 3.2.7.

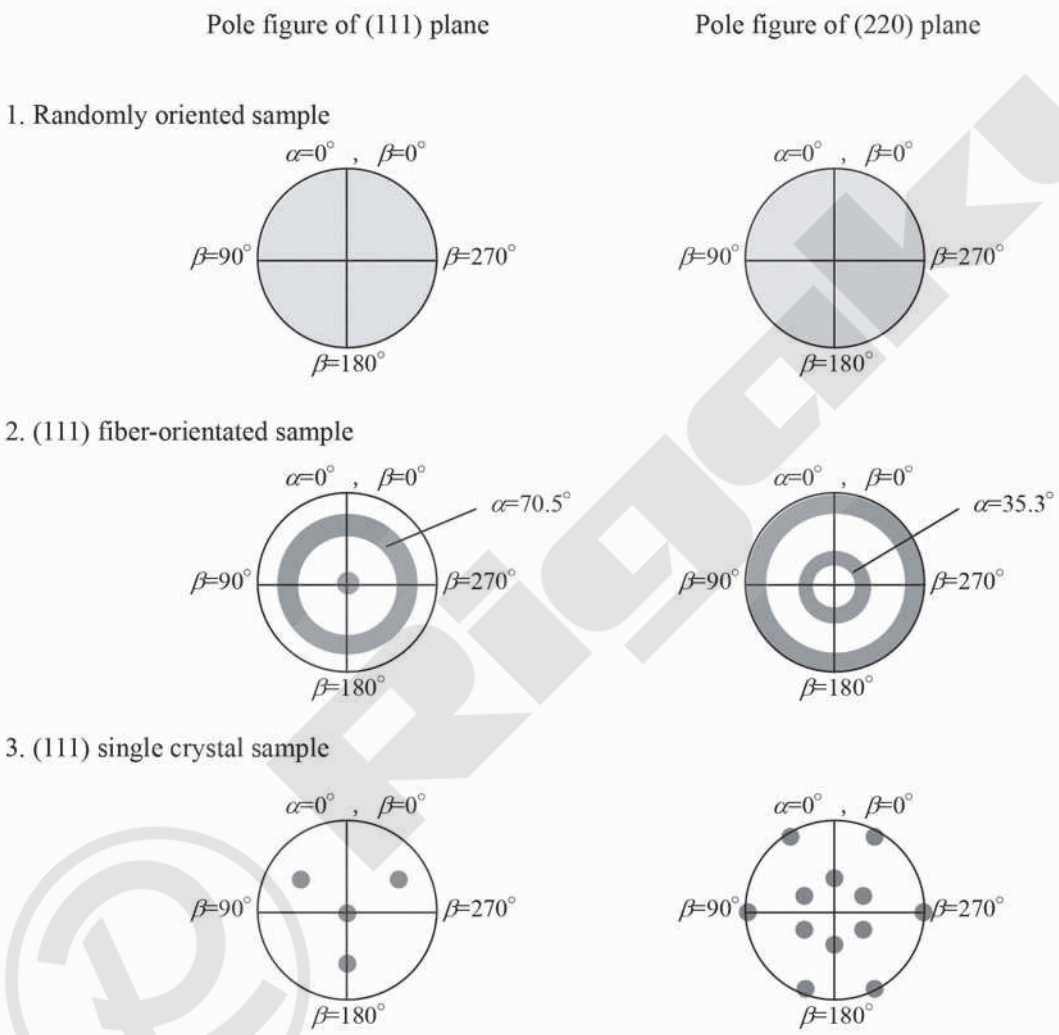

Figure 3.2.7. Examples of pole figures

3.2.5 Preferred Orientation and Crystallinity Measurement

Preferred orientation measurement measures a cross-section of a pole figure measurement. That is, it scans the α axis or the β axis and measures the spread (width) of the diffraction intensity distribution. The underlying principles are the same as for pole figure measurement. Here, the spread of the diffraction intensity is related to quantities such as the **degree of preferred orientation** or **mosaicity**.

The degree of preferred orientation is a term for expressing the amount of preferred orientation present in the sample compared to a randomly oriented sample. For example, in a randomly oriented sample, the diffraction intensity is uniformly distributed in the range β = 0° to 360°. In an oriented sample in which the diffraction intensity is observed in the range β = 81° to 109° and β = 261° to 279°, the degree of preferred orientation is calculated as follows: (spread of diffraction intensity)/360 = 36/360 = 10%.

Mosaicity is a term for the amount of fluctuation in orientation compared to a perfect single crystal. While mosaicity lacks a specific quantitative definition, if a perfect crystal does not show a spread in the diffraction intensity with width of 0° and a sample shows a spread in diffraction intensity from the center of ±0.5°, the crystal orientation of that sample can be regarded to fluctuate across a range of 1°. In this case, mosaicity can be expressed as 1°.

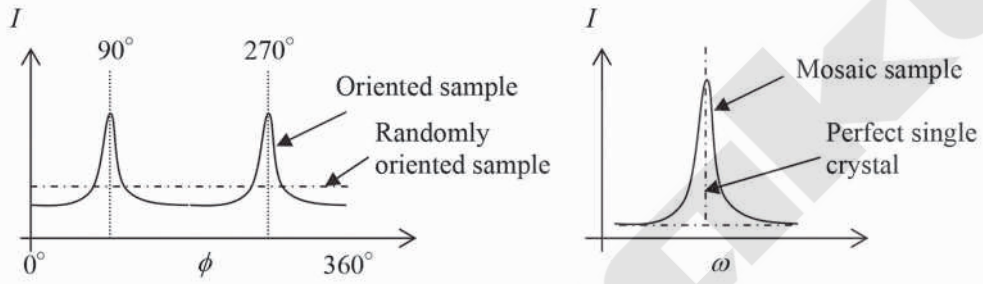

Figure 3.2.8. Degree of preferred orientation (left) and mosaicity (right)

3.2.6 Rocking Curve Measurement

Rocking curve measurement measures diffraction intensity distributions along a reciprocal lattice vector. As Fig. 3.2.9 shows, this measurement does not require the incident angle and exit angle of X-rays relative to the surface to be equal. It scans the $2\theta/\omega$ axis while maintaining a relationship in which a change in diffraction angle 2θ is always twice the change in incident angle ω. Since rocking curve measurement measures the diffraction intensity distribution along a reciprocal lattice vector, it can measure changes in interplanar spacing.

Rocking curve measurement is generally used to evaluate the thickness or mixed crystal ratio of an epitaxial film on a sample called a perfect crystal—i.e., one with extremely high crystallinity. Chapter 7 gives a detailed discussion of the principles underlying rocking curve measurement.

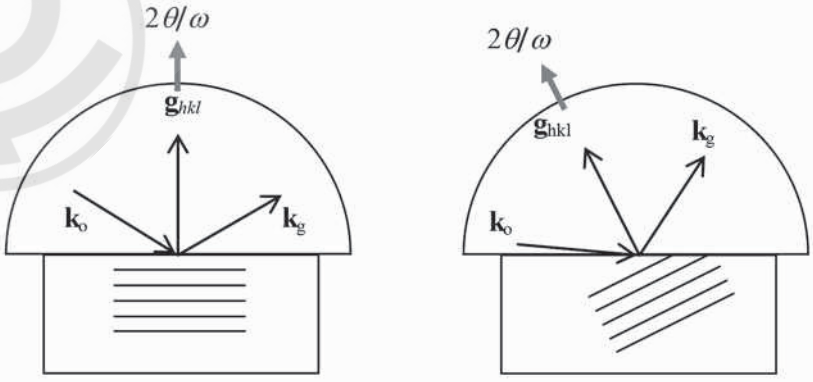

Figure 3.2.9. Schematic illustration of rocking curve measurement: (left) symmetric plane; (right) asymmetric plane

3.2 What Does Diffraction Measurement Observe?

3.2.7 Reciprocal Space Mapping (RSM) Measurement

Reciprocal space Mapping (RSM) measurement measures diffraction intensity distributions by scanning both the diffraction angle and sample rotation axes and plots the result in reciprocal space. As described in Chapter 2, the reciprocal lattice includes information on the crystal structure, crystal orientation relationships, crystallinity, and the preferred orientation of the sample investigated. The central coordinates, shapes, and positional relationships of the reciprocal lattice points appearing in the two-dimensional (or three-dimensional) data plotted in reciprocal space provide a wide range of information on crystal structure.

As Fig. 3.2.10 shows, RSM measurement measures the positions and shapes of reciprocal lattice points by scanning the 2θ and ω axes in the scattering plane as specified by the specific values for χ and ϕ. Three types of scanning methods are used: "ω step $2\theta/\omega$ scan," which repeats the $2\theta/\omega$ scan while gradually changing ω; "$2\theta/\omega$ step ω scan," which repeats the ω scan while gradually changing $2\theta/\omega$; and "mesh measurement," which scans the axes while maintaining constant step intervals in q coordinates.

A diffractometer capable of performing in-plane measurements can also perform in-plane reciprocal space mapping measurements. Two types of scanning methods are used: "ϕ step $2\theta\chi/\phi$ scan," which repeats the $2\theta\chi/\phi$ scan while gradually changing ϕ; and "$2\theta\chi/\phi$ step ϕ scan," which repeats the ϕ scan while gradually changing $2\theta\chi/\phi$.

When measurement is performed by a scanning method other than "mesh measurement," the angular position on each axis is converted into q coordinates using Formula 3.2.1 or Formula 3.2.2. A reciprocal space map plots the diffraction intensity in q coordinates in different colors.

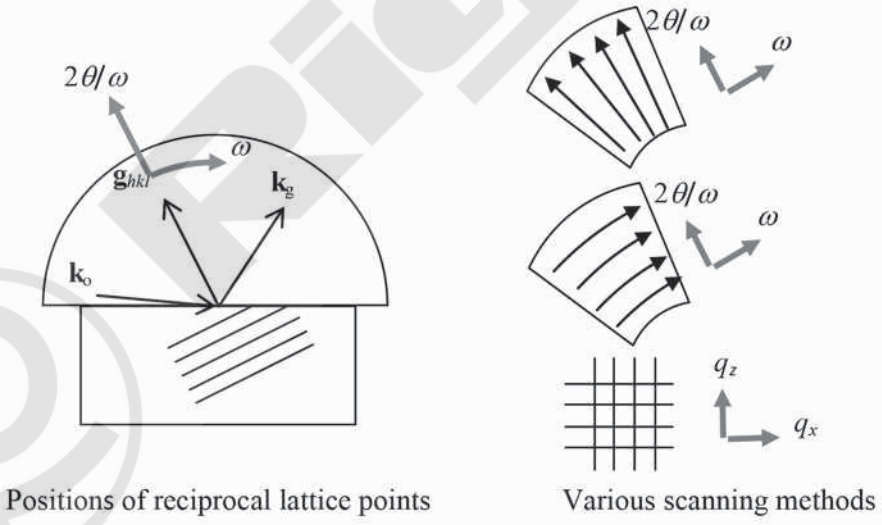

Figure 3.2.10. Schematic illustration of RSM measurement

Consider the example of a heteroepitaxial sample in which a cubic crystal film is epitaxially grown on a cubic crystal substrate. The film has lattice constants slightly greater than the substrate. If a beam diffracted from the film produces a distribution in the reciprocal lattice point centered at (q_x, q_y), it provides the following information:

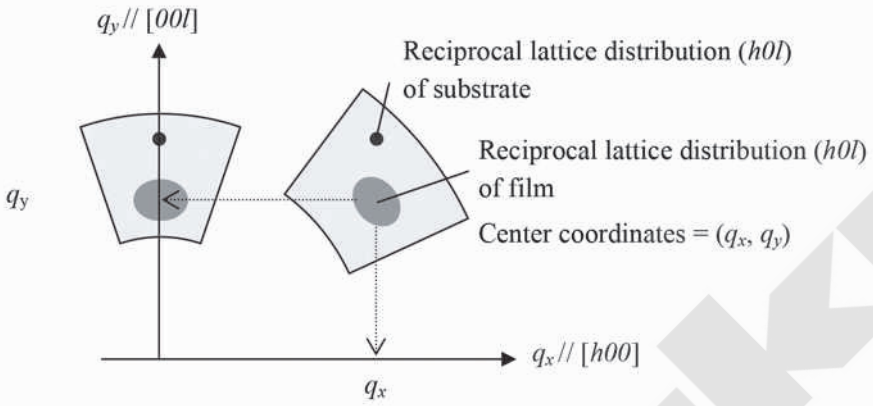

Figure 3.2.11. RSM map of (h0l) plane

- Information provided by the center coordinates of the reciprocal lattice distribution

  From the center coordinates of the reciprocal lattice, we can calculate interplanar spacing d. Since the length |q| of the reciprocal lattice vector is the inverse of d, the following formula holds:

$$d = \frac{1}{|q|} = \frac{1}{\sqrt{q_x^2 + q_y^2}}$$

Formula 3.2.1

  When q_x and q_y, the axes of the q coordinates, are parallel to crystallographic axes [*h00*] and [*00l*] of the sample, respectively, we can calculate d_{h00} and d_{00l} separately based on the values of the center coordinates (q_x, q_y) of the (*h0l*) reciprocal lattice distribution. The operation used to match the axes of the q coordinates with the crystallographic axes of the sample is performed as part of sample alignment in the measurement.

$$d_{h00} = \frac{1}{|q_x|},\ d_{00l} = \frac{1}{|q_y|}$$

Formula 3.2.2

  Multiplying the values of d_{h00} and d_{00l} by the Miller indices produces lattice constants a and c. In addition, if the reciprocal space map is similarly measured for the Miller indices in which k is not zero, we can also calculate lattice constant b. In this manner, we can determine the lattice constants and crystal system based on the results of RSM measurements for two or more Miller indices.

3.2 What Does Diffraction Measurement Observe?

- Information provided by spread of reciprocal lattice distribution

  If the crystallinity of the epitaxial film is less than that of the substrate, the reciprocal lattice point distribution will broaden. The direction in which the distribution broadens depends on the type of change in crystallinity. Fig. 3.2.12 illustrates this property.

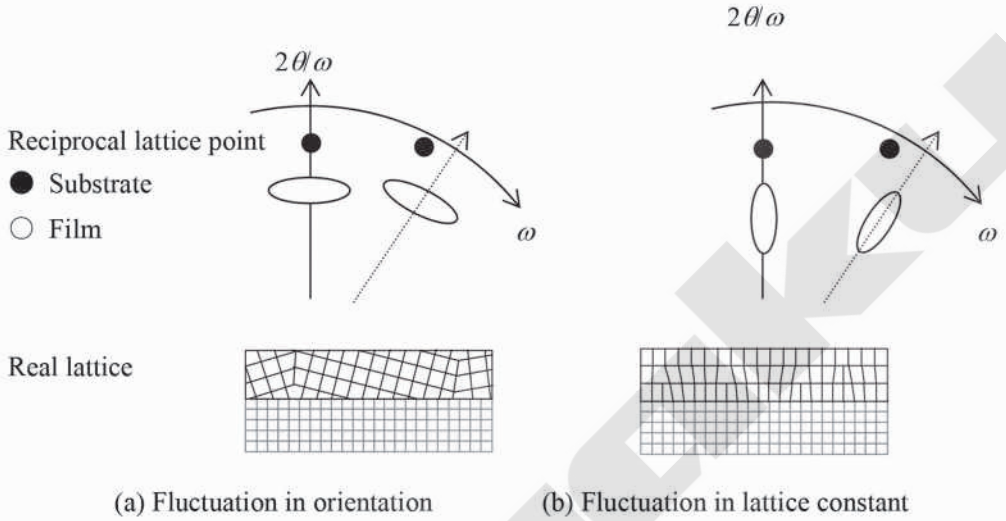

(a) Fluctuation in orientation (b) Fluctuation in lattice constant

Figure 3.2.12. Reciprocal space map of heteroepitaxial layer (crystallinity)

If the epitaxial film is a mosaic crystal or if the lattice is bent by stress, the crystal orientation fluctuates, and the reciprocal lattice points of the film spread in the ω direction (the direction of the arc of the RSM measurement range) with respect to that of the substrate as shown in Fig. 3.2.12 (a).

If the epitaxial film has a dislocation, parts with a mixture of relaxed and unrelaxed lattices, or variations in composition ratios, the lattice constants will fluctuate, and the reciprocal lattice points of the film will spread along the $2\theta/\omega$ direction (the radial axis of the RSM measurement range) with respect to that of the substrate, as shown in Fig. 3.2.12 (b).

- Information provided by relative positions with respect to reciprocal lattice points of substrate

  The relative positions of the reciprocal lattice points of the epitaxial film and the substrate change, depending on lattice matching and the presence or absence of lattice relaxation. Fig. 3.2.13 schematically illustrates the entire reciprocal space map.

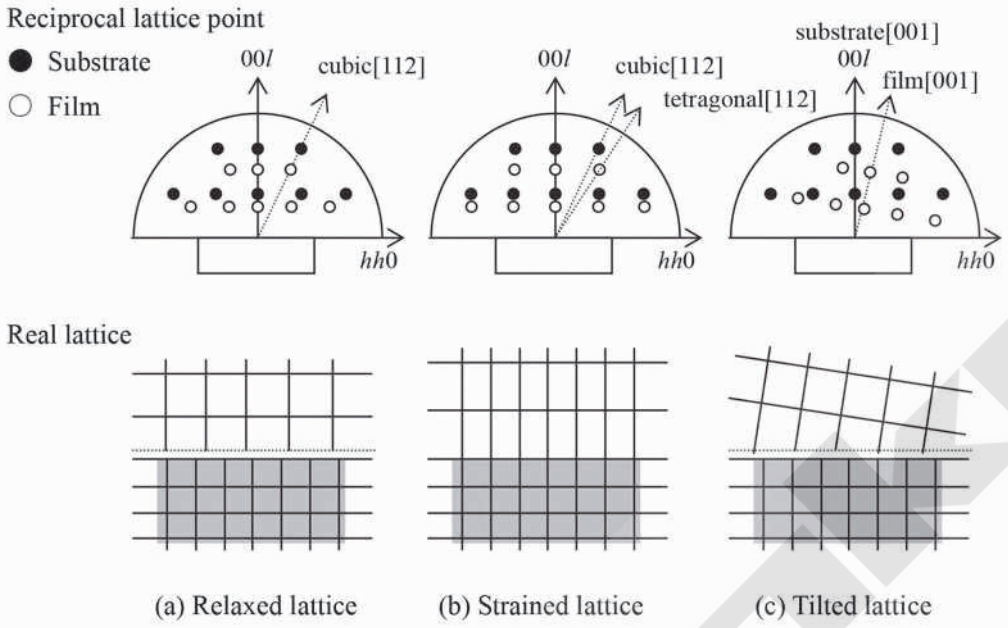

Figure 3.2.13. Reciprocal space map of heteroepitaxial layer (lattice relaxation)

The term lattice relaxation refers to the state of an epitaxial film having the same cubic crystal structure as the bulk of the material composing the film, as shown in Fig. 3.2.13 (a). In this case, the reciprocal lattice point of the film with the indices (*hkl*) is positioned on the line connecting the reciprocal lattice point (*hkl*) of the substrate and the origin of the reciprocal lattice—along the line of the $2\theta/\omega$ scan for both symmetric and asymmetric reflections.

If the lattice of the film is strained at the interface between the epitaxial film and the substrate in a manner such that the in-plane lattice constants (a and b in Fig. 3.2.13) of the epitaxial film and substrate match, the reciprocal lattice point of the film with the indices (*hkl*) is positioned directly below the reciprocal lattice point (*hkl*) of the substrate for both symmetric and asymmetric reflections, as shown in Fig. 3.2.13 (b). Here, for asymmetric reflections, the reciprocal lattice points of the substrate and the film are not positioned on the same line of the $2\theta/\omega$ scan. As Fig. 3.2.14 shows, the lattice of the film is strained to form a tetragonal crystal structure (a = b ≠ c), so that the (*hkl*) direction differs from that for the cubic crystal structure of the substrate.

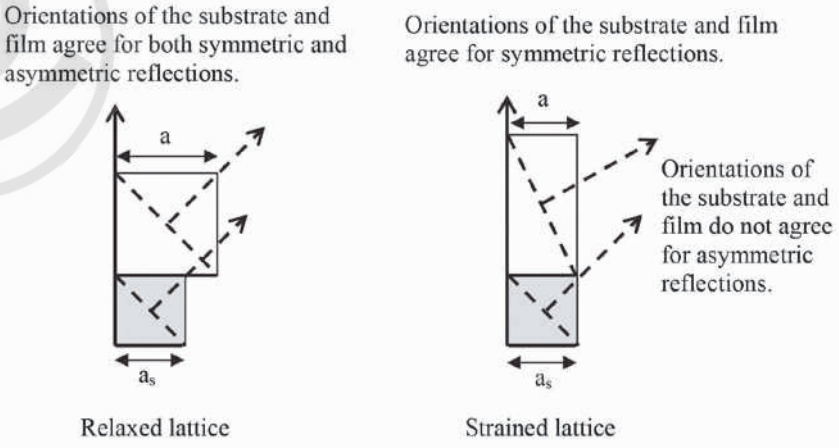

Figure 3.2.14. Asymmetric reflection of strained lattice

3.2 What Does Diffraction Measurement Observe?

Depending on the layer structure and heat treatment conditions of the epitaxial film, the interface may assume a state intermediate between the “relaxed lattice” and “strained lattice” indicated in Fig. 3.2.14. The degree of relaxation is expressed by the relaxation rate. The relaxation rate is calculated from the in-plane lattice constants of the substrate and epitaxial film. If we denote the lattice constant of the substrate as a_s, the lattice constant of the completely relaxed epitaxial film as a_0, and the lattice constant of the measurement sample as a, the relaxation rate is given by the following formula:

$$\text{Relaxation rate} = \frac{a - a_s}{a_0 - a_s} \times 100(\%)$$ *Formula 3.2.3*

For the “relaxed lattice,” $a = a_0$, and the relaxation rate is 100%. For the “strained lattice,” $a = a_s$, and the relaxation rate is 0%.

Regardless of the presence or absence of lattice relaxation, if the crystal orientation of the film (the direction of the c axis in Fig. 3.2.13) is tilted with respect to that of the substrate, the reciprocal lattice points of the film will shift relative to the reciprocal lattice points of the substrate based on the tilt. The amount of shift corresponds to the shift in crystal orientation between the substrate and the film and equals the shift in reciprocal lattice points for the symmetric reflection.